Communication

A Parallel Block Preconditioner-Based VIE-FFT Algorithm for Modeling the Electromagnetic Response From Nanostructures

Chengnian Huang and Wei E. I. Sha

***Abstract*— The superior ability of nanostructures to manipulate light has propelled extensive applications in nanoelectromagnetic components and devices. Computational electromagnetics plays a critical role in characterizing and optimizing the nanostructures. In this work, a parallel block preconditioner-based volume integral equation (VIE)-fast Fourier transform (FFT) algorithm is proposed to model the electromagnetic response from representative nanostructures. The VIE using uniform Cartesian grids is first built, and then the entire volumetric domain is partitioned into geometric subdomains based on the regularity and topology of the nanostructure. The block diagonal matrix is thus established, whose inverse matrix serves as a preconditioner for the original matrix equation. The resulting linear system is solved by the biconjugate gradient-stabilized (BiCGSTAB) method with different residual error tolerances in the inner and outer iteration processes and the FFT algorithm is used to accelerate the matrix–vector product (MVM) operations throughout. Furthermore, because of the independence between the inner processes of solving block matrix equations, the OpenMP framework is employed to execute the parallel operations. Numerical experiments indicate that the proposed method is effective and reduces both the iteration number and the computational time significantly for representative nanoelectromagnetic problems like the dielectric focusing metasurfaces and the plasmonic solar cells.**

***Index Terms*— Block preconditioner, fast Fourier transform (FFT), nanostructures, OpenMP, volume integral equation (VIE).**

I. Introduction

Nanostructures serve as the fundamental building blocks for nanoelectromagnetic designs and hold significant importance in emerging engineering applications, such as virtual/augmented reality [1], metalens [2], organic solar cells (OSCs) [3], photonic integrated circuits [4], and so on. Computational electromagnetics plays a vital role in characterizing and optimizing nanostructures, effectively reducing the costs and time associated with realistic experimental fabrication. In particular, the accurate modeling of light–matter interaction within nanostructures is essential. This modeling endeavor aims to propel the exploration of novel physical effects and their corresponding experimental investigation. Numerous research studies have been conducted to address categories of nanostructure problems, such as the planar plasmonic structures [5], complex disordered stacks of gold nanorods or 3-D photonic crystals [6], the nonlinear optical process of metal nanoparticles [7], and so on. In this work, the focusing metasurfaces and the plasmonic solar cells are chosen as representative examples, which possess commonly used structural features that display far-field interference and near-field coupling effects, respectively.

Manuscript received 8 July 2022; revised 19 September 2023; accepted 27 October 2023. Date of publication 21 November 2023; date of current version 9 February 2024. This work was supported by the National Natural Science Foundation of China under Grant 61975177 and Grant U20A20164. *(Corresponding author: Wei E. I. Sha.)*

The authors are with the College of Information Science and Electronic Engineering, Zhejiang University, Hangzhou 310027, China (e-mail: 12031047@zju.edu.cn; weisha@zju.edu.cn).

Color versions of one or more figures in this communication are available at https://doi.org/10.1109/TAP.2023.3331512.

Digital Object Identifier 10.1109/TAP.2023.3331512

Considering the dimensions and material composition of nanostructures, there are three kinds of popular rigorous methods including the differential equation (DE)-based methods, the integral equation (IE)-based methods, and the semianalytical methods. The semianalytical methods can only solve the electromagnetic response for specific nanostructures. The DE methods involving the finite-difference time-domain (FDTD) method [8], the finite-difference frequency-domain (FDFD) method [9], and the finite-element method (FEM) [10] discretize the whole region, resulting in a large number of unknowns to be solved. Moreover, the accuracy of modeling high-contrast plasmonic structures with strong evanescent wave coupling is reduced due to the dispersion error in both the FEM and the FDTD method, as well as the staircase approximation used in the FDTD method [11]. Differently, the IE methods only need to discretize the object. Not only is the number of unknowns small, but also the radiation boundary condition can be satisfied automatically by using the dyadic Green's function. They usually have higher accuracy. Because nanostructures often exhibit complex and intricate geometries including sharp edges, corners, fine details, and so on, some of which involve open surfaces, the IE methods are the superior option compared with the DE methods. The IE methods are classified into the surface IE (SIE) method [12] and the volume IE (VIE) method [13]. For the metallic, homogeneous dielectric, and composite metallic and dielectric objects, the SIE is preferred to be established at the surface of the nanostructure [14], but the precorrected-fast Fourier transform (FFT) algorithm [15] is required for the near-field calculations. In comparison, the VIE in conjunction with the method of moments (MoMs) [16] is an easy-to-implement and flexible method to calculate the electromagnetic scattering from dielectric bodies of arbitrary shape and inhomogeneous material composition [17]. Although for some scattering structures, the impedance matrix can be poorly conditioned and the conventional MoM suffers from tremendously high computational cost and memory requirement, efficient iterative and fast algorithms have alleviated this problem to some extent.

In recent years, many efforts have been made to apply various iterative and fast algorithms to reduce the complexity and memory cost of the MoM solution. The commonly used iterative approach to solve the VIE is the biconjugate gradient-stabilized (BiCGSTAB) method [18] from the Krylov subspace family. The Krylov methods require the computation of some matrix–vector product (MVM) operations at each iteration, which accounts for the major computational cost of this class of methods. However, by performing the MVM with the 3-D FFT [19], the computational complexity and the memory use are reduced to $O(N \log N)$ and $O(N)$, respectively. Normally, the FFT algorithm requires the volume of the object to be discretized into uniform hexahedral cells to use the Toeplitz property of the impedance matrix, which results in a large number of unknowns for an accurate geometric model with the staircase approximation. However, near-field calculation without precorrection can save a great amount of computer resources, especially for nanoelectromagnetic problems involving strong near-field interactions that cover a large

range. There is another problem that the typical MoM implementations for dielectric bodies do not consider the induced currents flowing between the dielectric volumes and the free space, which has been discussed in [20]. However, this work primarily focused on capturing the field interaction effect of unit cells, manipulating an efficient preconditioner, and conducting further studies on the accuracy and efficiency of the proposed preconditioned solver. More extensions of this problem will be made in our future work.

To accelerate the convergence rate of the Krylov method, substantial efforts have been devoted to the development of straightforward preconditioners. The commonly adopted preconditioning tools include the incomplete LU factorization [21] and the symmetric successive overrelaxation (SSOR) [22], both of which are difficult to implement in parallel. Therefore, we propose a combination of parallel computing techniques and an efficient block preconditioning method inspired by the rank-revealing decomposition preconditioner [23], which is well-suited for the organized unit nanostructures. Based on the fact that the spectral properties of the impedance matrix are mainly determined by the near-field dependence of the IE kernel especially for nanoelectromagnetic applications [24], the entire volumetric domain is partitioned into some geometric subdomains. As a result, a block diagonal matrix resulting from the local geometries of near-field interactions is established to serve as an approximation of the original impedance matrix. The inversion of the approximate matrix is referred to as a preconditioner, and the process requires solving the block matrix equations simultaneously. Therefore, the BiCGSTAB-FFT method is once again adopted to solve the submatrix equations in the inner iterations, combined with the OpenMP parallel technique for loops in the outer iterations.

In this communication, the theory of the preconditioned VIE-FFT algorithm is described in Section II. In Section III, two commonly encountered regular nanostructures are provided to demonstrate the correctness and efficiency of the proposed method. Finally, the conclusion is given in Section IV.

II. Theory

A. VIE-MoM

Here, we consider an inhomogeneous 3-D nanostructure illuminated by a plane wave at a specific frequency of interest. $\boldsymbol{E}^s$ is the corresponding scattered field due to the induced volumetric polarization current $\boldsymbol{J}^s$ as follows [25]:

$$\begin{aligned}\boldsymbol{E}^s &= -j\omega\mu_0 \int_V g\left(\boldsymbol{r},\boldsymbol{r}'\right)\boldsymbol{J}^s\left(\boldsymbol{r}'\right)dv' \\ &\quad + \frac{1}{j\omega\varepsilon_0}\int_V \nabla\nabla g\left(\boldsymbol{r},\boldsymbol{r}'\right)\cdot\boldsymbol{J}^s\left(\boldsymbol{r}'\right)dv' \\ &= -j\omega\mu_0 \int_V \overleftrightarrow{\mathbf{G}}\left(\boldsymbol{r},\boldsymbol{r}'\right)\cdot\boldsymbol{J}^s\left(\boldsymbol{r}'\right)dv' \end{aligned} \tag{1}$$

where $g(\boldsymbol{r},\boldsymbol{r}') = e^{-jk|\boldsymbol{r}-\boldsymbol{r}'|}/4\pi|\boldsymbol{r}-\boldsymbol{r}'|$ denotes the scalar Green's function in free space, $\overleftrightarrow{\boldsymbol{G}}$ denotes the corresponding dyadic Green's function, and $\boldsymbol{r}$ and $\boldsymbol{r}'$ are the observation and source point locations, respectively. The permittivity and permeability in free space are denoted by ε_0 and μ_0, respectively.

According to the relation between the polarization current and the electric polarization vector, the total electric field could be described by $\boldsymbol{J}^s$ as

$$\boldsymbol{E}^{\text{tot}} = \frac{\boldsymbol{J}^s(r)}{j\omega\left(\varepsilon-\varepsilon_0\right)}. \tag{2}$$

The total electric field is the summation of the incident field and the scattered field, and thus the VIE can be written as

$$\boldsymbol{E}^{tot} = \boldsymbol{E}^{inc} + \boldsymbol{E}^s. \tag{3}$$

Based on the equations above, one can explicitly write the equation with the unknown $\boldsymbol{J}^s$ as

$$\frac{\boldsymbol{J}^s(\boldsymbol{r})}{j\omega\left(\varepsilon-\varepsilon_0\right)} + j\omega\mu_0\int_V \overleftrightarrow{\boldsymbol{G}}\left(\boldsymbol{r},\boldsymbol{r}'\right)\cdot\boldsymbol{J}^s\left(\boldsymbol{r}'\right)dv' = \boldsymbol{E}^{inc}. \tag{4}$$

Here, the MoM is used to discretize the equation. The unknown volumetric currents can be expanded into sets of basis functions, and then the problem is converted to minimize the associated residual errors with sets of weighting or testing functions [26]. Considering our examples have regular geometries that allow low cost and easy fabrication, a hexahedron mesh is utilized to discretize the volumetric structure, enabling fast MVM and efficient preconditioning. The unknown currents are expanded into rooftop basis functions

$$\boldsymbol{J}^s = \sum_{i=1}^{3}\boldsymbol{p}_i\sum_{k=0}^{N_1}\sum_{m=0}^{N_2}\sum_{n=0}^{N_3}J_i^D(kmn)T_{kmn}^s. \tag{5}$$

$\boldsymbol{p}_i$ are the direction vectors, J_i^D are the coefficients of current basis functions, and T_{kmn}^s are the volumetric rooftop functions. Then, the pulse function is applied to test the equation. Considering the Cartesian coordinate system, all three polarization x-, y-, and z-components of the unknown currents are taken into account. The above equation can be transformed into the matrix equation

$$\underbrace{\begin{pmatrix} L_{xx} & L_{xy} & L_{xz} \\ L_{yx} & L_{yy} & L_{yz} \\ L_{zx} & L_{zy} & L_{zz}\end{pmatrix}}_{A}\underbrace{\begin{pmatrix} J_x^s \\ J_y^s \\ J_z^s\end{pmatrix}}_{x} = \underbrace{\begin{pmatrix} E_x^{inc} \\ E_y^{inc} \\ E_z^{inc}\end{pmatrix}}_{b} \tag{6}$$

where

$$L_{ij} = \begin{cases} L_{ii}^c + L_{ii}^q, & \text{for } i = j \\ L_{ij}^q, & \text{for } i \neq j \end{cases} \tag{7}$$

$L_{ii}^c J_i^s$ and $L_{ij}^q J_i^s$ are defined as

$$L_{ii}^c J_i^s = \frac{J_i^s(\boldsymbol{r})}{j\omega\left(\varepsilon-\varepsilon_0\right)} - j\omega\mu_0\int_v J_i^s\left(\boldsymbol{r}'\right)g\left(\boldsymbol{r},\boldsymbol{r}'\right)dv' \tag{8}$$

$$L_{ij}^q J_i^s = \frac{1}{j\omega\varepsilon_0}\frac{\partial}{\partial u_i}\int_v \frac{\partial J_j^s\left(\boldsymbol{r}'\right)}{\partial u_j'}g\left(\boldsymbol{r},\boldsymbol{r}'\right)dv'. \tag{9}$$

B. Preconditioned Iterative Solver

Discretizing the VIE with MoM, a dense impedance matrix $\boldsymbol{A}$ will be generated as shown in (6). Considering the symmetry of the linear system, some algorithms like the GMRES [27], the CGS [28], and the BiCGSTAB are all applicable, which have low memory cost and good convergence properties as well. Besides, they are easy to combine with a preconditioner. In this work, the BiCGSTAB method is employed as a proof of principle, which shows good performances combined with the parallel block preconditioner. The formulation is equivalent to applying the BiCGSTAB method to the explicitly preconditioned system: $\widetilde{\boldsymbol{A}}\widetilde{\boldsymbol{x}} = \widetilde{\boldsymbol{b}}$, where $\widetilde{\boldsymbol{A}} = \boldsymbol{K_1^{-1}}\boldsymbol{A}\boldsymbol{K_2^{-1}}$, $\widetilde{\boldsymbol{x}} = \boldsymbol{K}_2\boldsymbol{x}$, and $\widetilde{\boldsymbol{b}} = \boldsymbol{K}_1^{-1}\boldsymbol{b}$. We consider a right preconditioner, which means that $\boldsymbol{K}_1$ is the unit matrix, and $\boldsymbol{K}_2$ is an approximation of the impedance matrix $\boldsymbol{A}$. In the outer iteration process, two extra matrix equations $\boldsymbol{y} = \boldsymbol{K}_2^{-1}\boldsymbol{p}_i$ and $z = \boldsymbol{K}_2^{-1}\boldsymbol{s}$ need to be solved, where $\boldsymbol{y}$, $\boldsymbol{p}_i$, z, and $\boldsymbol{s}$ correspond to the vectors involved in this process. To reduce computational complexity, we explore the structure for constructing the block preconditioners, that is to say, $\boldsymbol{K}_2\boldsymbol{x} = \boldsymbol{b}$ (representing the two extra equations above) could be approximately viewed as solving the combination of matrix equations of divided blocks, for example, $\boldsymbol{A}_1\boldsymbol{x} = \boldsymbol{b}_1$, $\boldsymbol{A}_2\boldsymbol{x} = \boldsymbol{b}_2$, and so on. Since the interaction between blocks is not considered, only the diagonal of the large matrix has

nonzero values. The extra matrix equation to be solved is given as follows:

$$\begin{pmatrix} \boldsymbol{A}_1, 0, \ldots \\ 0, \boldsymbol{A}_2, \ldots \\ \ldots\ldots\ldots \\ 0, \ldots, \boldsymbol{A}_N \end{pmatrix} \begin{pmatrix} \boldsymbol{J}_1 \\ \boldsymbol{J}_2 \\ \vdots \\ \boldsymbol{J}_N \end{pmatrix} = \begin{pmatrix} \boldsymbol{b}_1 \\ \boldsymbol{b}_2 \\ \vdots \\ \boldsymbol{b}_N \end{pmatrix}. \tag{10}$$

In view of the vector current and the interaction of currents along the three directions, matrices including coefficients of the interactive x-, y-, and z-components are established. Here is an example of the impedance matrix for a divided block

$$\boldsymbol{A}_1 = \begin{pmatrix} A_{1\times1x}, & \ldots, & A_{1xnx}, & A_{1\times1y}, & \ldots, & A_{1\times1z}, & \ldots \\ \vdots & & & & & & \\ A_{nx1x}, & \ldots, & A_{nxnx}, & A_{nx1y}, & \ldots, & A_{nx1z}, & \ldots \\ A_{1y1x}, & \ldots, & A_{1ynx}, & A_{1y1y}, & \ldots, & A_{1y1z}, & \ldots \\ \vdots & & & & & & \\ A_{ny1x}, & \ldots, & A_{nynx}, & A_{ny1y}, & \ldots, & A_{ny1z}, & \ldots \\ A_{1z1x}, & \ldots, & A_{1znx}, & A_{1z1y}, & \ldots, & A_{1z1z}, & \ldots \\ \vdots & & & & & & \\ A_{nz1x}, & \ldots, & A_{nznx}, & A_{nz1y}, & \ldots, & A_{nz1z}, & \ldots \end{pmatrix}. \tag{11}$$

The coefficients of x-components in the dotted box correspond to the operator L_{xx} in (6), which represent the contribution of the currents of x-components to the electric fields of x-components, likewise for the y- and z-components. For a divided block, solving the submatrix equation is an inner iteration process, which also uses the BiCGSTAB-FFT method. Because only the approximate inverse of matrix $\boldsymbol{A}$ needs to be considered, the submatrix equation in (10) can be solved with a larger residual error, that is, the stopping criteria of iteration can be softened. After retaining the newly solved current vector of the corresponding block, all currents are arranged into a new vector to continue the outer iteration process. Notably, since the interaction between blocks is not considered, data exchange between different blocks is not necessary, which is ideal for parallel computing. The OpenMP parallelization paradigm provides a multithread capacity and fully makes use of the features of shared memory [29], which executes multiple threads for loops of solving block matrix equations. In general, the number of threads is often comparable to the number of divided blocks. It is clear that if there are more blocks to be divided, the time to solve the matrix equation for each block will be shortened. Nevertheless, the use of smaller-sized diagonal block matrices leads to a poorer approximation of the matrix $\boldsymbol{A}$, thus hindering the efficiency of the outer iteration process. Evidently, the division of blocks significantly influences the efficiency of the outer iteration, resulting in a tradeoff between the time required for the solution of submatrix equations in one iteration and the number of outer iteration steps.

III. Numerical Results

In this section, some numerical results are shown to illustrate the effectiveness of the VIE-FFT algorithm with the preconditioner. First, to verify the accuracy of the algorithm precisely, we consider the scattering of a dielectric sphere and a metallic sphere with the radius of $r = 400$ nm (5 832 000 unknowns at 750 THz). The relative permittivity of the dielectric material is 2.25 corresponding to the refractive index of $n = 1.5$. The complex permittivity of the metallic material is $\epsilon_r = -1.05 - j5.62$. The comparison to the Mie series solution [30] is made for the radar cross section (RCS) of the sphere as plotted in Figs. 1 and 2. The relative L2-norm errors of the E-plane RCS are 2.5% and 3.75%, respectively. It can be found that there is an excellent agreement between them.

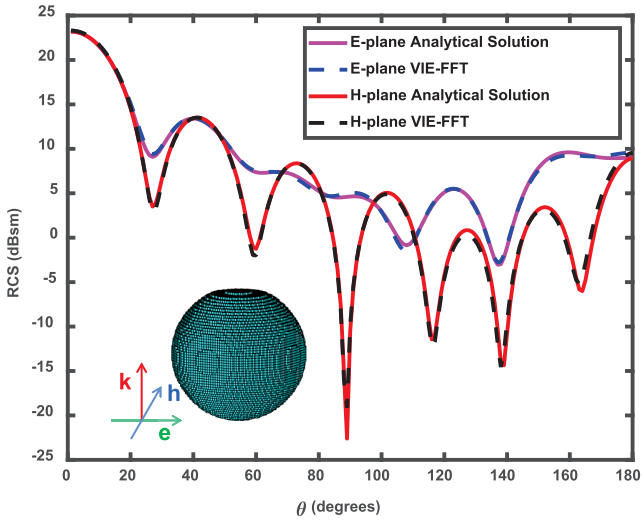

Fig. 1. Bistatic RCS of a dielectric sphere with the radius of $r = 400$ nm at 750 THz ($\epsilon_r = 2.25$).

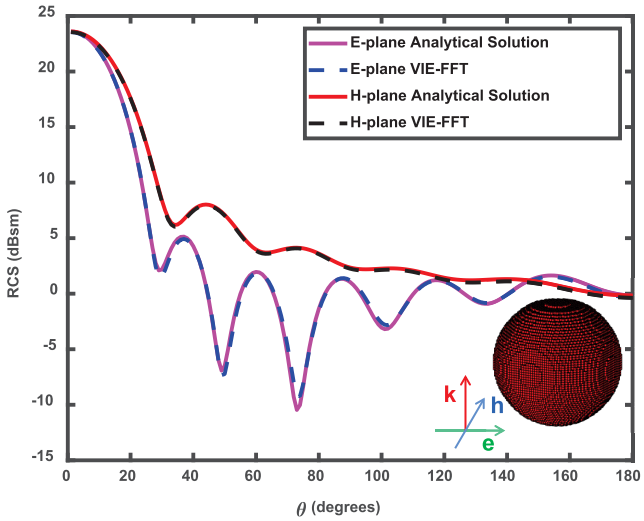

Fig. 2. Bistatic RCS of a metallic sphere with the radius of $r = 400$ nm at 750 THz ($\epsilon_r = -1.05 - j5.62$).

Next, we investigate the performance of the preconditioned algorithm for modeling the electromagnetic response from two examples of nanostructures, which are performed with an IBM server of 256 GB memory.

A. Focusing Dielectric Metasurfaces

The electromagnetic metasurface is a useful structure to control beam propagation by phase tailoring. To reduce the loss at optical frequencies and increase the feasibility of fabrication, extensive studies have been conducted on the dielectric-only metasurfaces. Here, the resonating disk as a unit cell is made of silicon with the permittivity of $\epsilon_r = 12.25$, placed onto a substrate of $\epsilon_r = 2.25$. The thicknesses of Si and SiO_2 are 250 and 25 nm, respectively. The schematic of the cylinder is displayed in Fig. 3(a). Then, we study the transmission phase of the disk as a function of radius, where the working frequency is fixed at 214 THz. As shown in Fig. 3(b), the

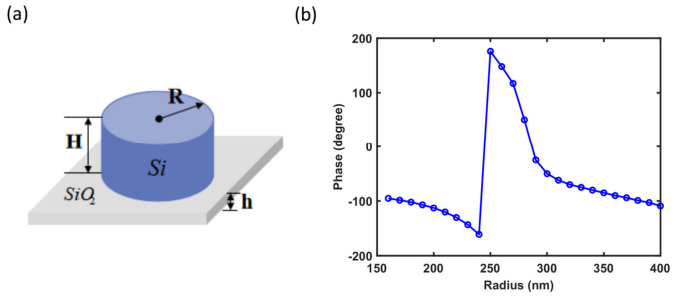

Fig. 3. Change of transmission phase with variation of cylinder's radius. (a) Schematic of single Si cylinder with substrate of SiO_2: $H = 250$ nm, $h = 25$ nm. (b) Diagram of phase change.

complete 360° transmission phase is covered while the radius ranges from 160 to 400 nm. According to the phase profile settings

$$\Phi(x, y) = k_{SiO_2}\left(\sqrt{x^2 + y^2 + d^2} - d\right) \tag{12}$$

where k_{SiO_2} is the wavenumber in the dielectric, x and y are the coordinate positions of the units on the plane, d is the focal length, and the size of the unit cell is 900 nm. A metasurface for plane-wave focusing could be designed by arranging the disks of different sizes at a fixed focal length. The structure is designed to length × width × height as $16\lambda_0 \times 16\lambda_0 \times 0.2\lambda_0$ (λ_0 is the wavelength of free space) and creating 47 grids per λ_0 (considering high dielectric contrast), incident wave is polarized along the x-direction, and the focal length d is set to 10λ, that is, 14 μm. So, the total number of mesh elements is 6 187 500 and that of unknown currents along the three dimensions is 18 562 500. Nearly 6 GB of memory cost is required. To employ the parallel block preconditioner, we divide the structure evenly into blocks based on its regularity of arrangements. The residual error of the outer iteration is set to 0.001, whereas the inner residual error for the stopping criteria of preconditioning is 0.01. In Fig. 4, the distribution of the electric-field amplitude in the x–z propagation plane is shown, along with the results simulated by the commercial software CST. The performance of convergence is also displayed. A relatively small number of iterations are needed for the proposed method, whereas the original un-preconditioned VIE-FFT algorithm fails to converge to $\epsilon = 10^{-3}$ within 1000 iterations. To validate the accuracy of results quantitatively, the normalized electric-field amplitude of the vertical cut of the focusing spot size at $x = 0$ is compared in Fig. 5. We can see that the field results from the VIE method and the FDTD method of CST are in good agreement. They produce the accurate focusing position at 14 μm as the theoretical design, whereas the focusing position calculated by the FEM of CST slightly shifts. In addition, the electric-field amplitude calculated by CST shows instability near the focusing position, which might contribute to the error to some extent. Therefore, the convergence property is studied to re-examine the reliability of the proposed method. The structure is discretized with different cell sizes (12.5, 25, and 50 nm, $\Delta x = \Delta y = \Delta z$). As the grid size decreases from 50 to 12.5 nm, equivalently, the number of grids increases from 1 215 000 to 71 280 000. We take the results simulated by the FDTD method of CST with a finer grid as the reference, then compute corresponding relative L2-norm errors as depicted in Fig. 6. It can be observed that the error becomes smaller as the grid size decreases, which demonstrates the stability and accuracy of the method. Evidently, sufficient mesh cells are required for good convergence. Furthermore, Table I shows the total calculation time of different methods. We can see that compared to the FDTD method, the FEM and the unpreconditioned VIE method are slower.

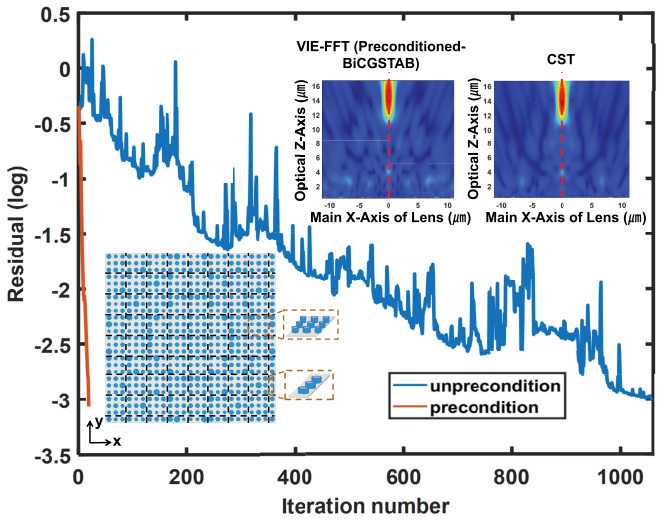

Fig. 4. Residual error versus iteration number for the metasurface. The inset shows the simulated intensity profiles by the preconditioned VIE-FFT algorithm and CST software.

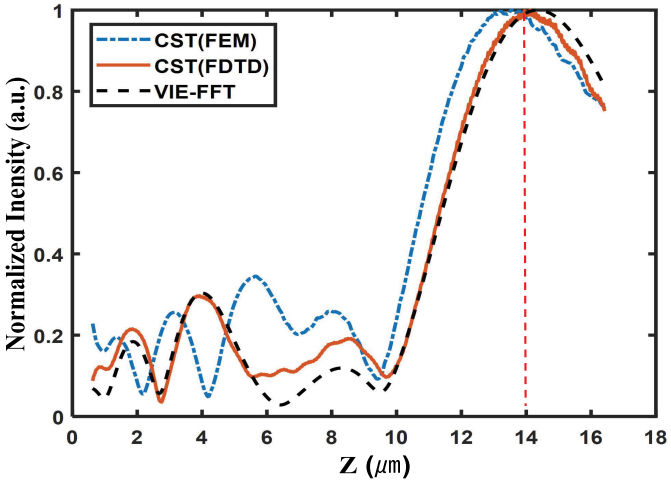

Fig. 5. Normalized electric-field amplitude of the vertical cut of the focusing spot size at $x = 0$ by the proposed algorithm and CST software. The focal plane of the metasurface is designed to be $d = 14$ μm.

TABLE I
COMPUTATIONAL STATISTICS OF METASURFACE WITH THE RESIDUAL ERROR $\epsilon = 10^{-3}$

Number of units	CPU time			
	CST (FEM)	CST (FDTD)	VIE method	preconditioned VIE method
25 × 25	9 h 46 min 47 s	5 h 6 min 10 s	10 h 28 min 39 s	3 h 35 min 13 s

After introducing the preconditioner, the overall CPU time is roughly reduced to one-third of the unpreconditioned one. Compared with the CST, the proposed preconditioned method shows a substantial speedup. We have also tried alternative ways of divisions and find that there is no significant difference in the CPU time except for the slight speed improvement brought by the finer division of blocks, which would be attributed to the electric and magnetic resonance modes dominated by the strong dipole moment located in the center of the nanopillar [31]. The field information contained in each block is rich enough to represent the characterization of the whole matrix.

B. Plasmonic Solar Cells

The OSCs are promising for future green energy applications. Considering the low carrier mobility and the short exciton diffusion

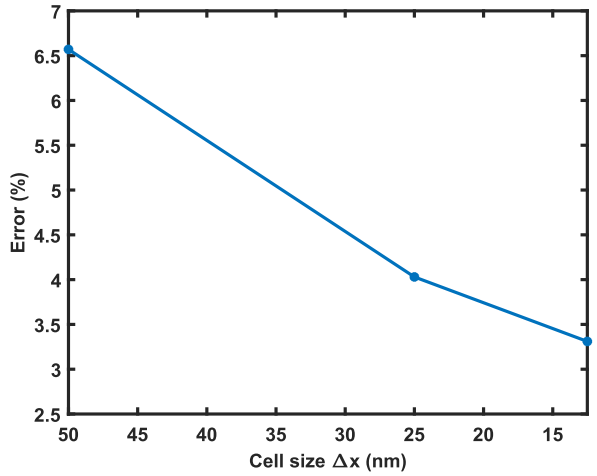

Fig. 6. Convergence of the preconditioned VIE-FFT algorithm: the relative L2-norm errors with different cell sizes (12.5, 25, and 50 nm). The solution of the FDTD method of CST is taken as the numerical reference.

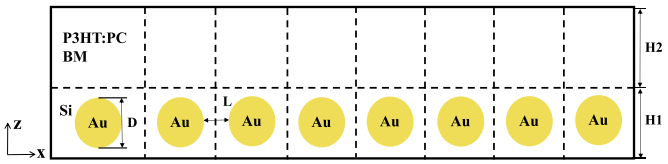

Fig. 7. Schematic of plasmonic solar cells with uniform blocks.

length, metallic nanoparticles are embedded into OSCs for enhancing the optical absorption on the basis of local plasmon resonance [32]. As displayed in Fig. 7, eight identical gold nanoparticles ($\epsilon_r = -8.45 - j1.41$) are incorporated into a silicon spacer, which is illuminated by an x-polarized wave along the z-axis at 500 THz. The diameter of the nanoparticle is $D = 60$ nm, and the particle–particle spacing is $L = 20$ nm. The thicknesses of the spacer (silicon) and the organic active layer (P3HT:PCBM) are $H1 = 80$ nm and $H2 = 120$ nm, respectively. Different from the dielectric metasurface, strong near-field evanescent wave coupling exists between the nanoparticles, which significantly slows down the iteration process. Here, we study the performances of the preconditioner under the two cases of vertical incidence and oblique incidence with different ways of division. The results are shown in Table II. To realize parallelization, the whole structure is divided into different longitudinal sections based on the regularity and topology. Considering the high dielectric contrast between the organic layer and the spacer, division along the interface of media is also studied. The inner residual error for the stopping criteria of preconditioning is set to 0.03. The residual error of iteration and the distribution of the electric field are displayed in Fig. 8, and a strong plasmon coupling between nanoparticles is clearly observed. The inset shows the near-field distribution for: 1) vertical incidence and 2) oblique incidence. From Table II, it is obvious that the block preconditioner works well in the two cases. In case 1) the near-field energy scattered from the metal nanoparticles is mainly distributed along the polarization direction (x-direction) of the incident field based on the wave physics of the local plasmon. When we try to divide more blocks along the x-direction and maintain the same number of blocks along the z-direction, according to the analysis of the tradeoff in Section II Part B, less field information will be contained in each block leading to coarse approximation, which increases the iteration steps. However, the reduced calculation time of submatrix equations for smaller blocks exceeds the time consumed by the increased iteration steps, achieving better preprocessing results. Similarly, in case 2), only a relatively small amount of

TABLE II
COMPUTATIONAL STATISTICS OF OSCS WITH THE RESIDUAL ERROR $\epsilon = 10^{-3}$

Method (i,ii)	Steps (i)	CPU time (i)	Steps (ii)	CPU time (ii)
original	247	34 min 12 s	276	35 min 35 s
x-4blocks and z-2blocks	12	29 min 15 s	16	34 min 25 s
x-8blocks and z-2blocks	19	20 min 32 s	16	18 min 59 s
x-8blocks	12	34 min 35 s	11	39 min 56 s

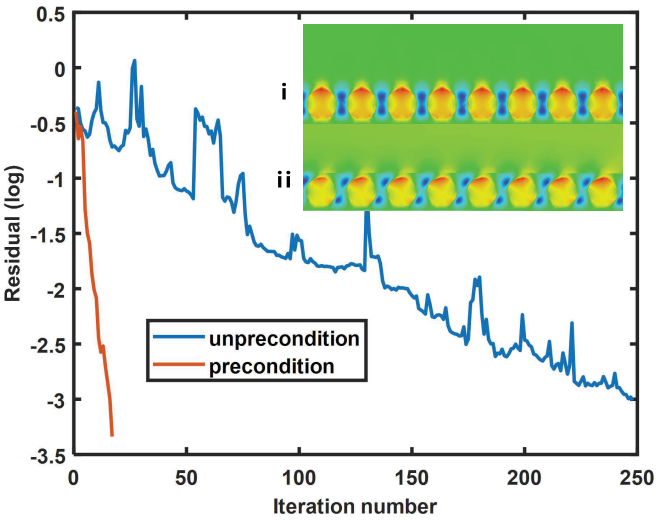

Fig. 8. Residual error versus iteration number for the OSCs.

TABLE III
COMPARISON OF CPU TIME BETWEEN SERIAL AND PARALLEL IMPLEMENTATIONS

Example	CPU TIME		Cores
	Serial	Parallel	
submatrix equations in (10)	69 min	5 min	30
one MVM by FFT	30 s	18 s	30

energy penetrates the active layer, which could be explained by the R^{-3} decay of the electric field and the reflection by the interface [33]. The local fields near the nanoparticles are fully contained in the corresponding blocks, that is the reason why the iteration steps are not reduced when the number of blocks along the x-direction is different. However, the calculation time is reduced a lot due to the simplicity of solving the equation for smaller blocks. Therefore, we conclude that the small blocks capture field information well and therefore make the preconditioning more effective. When comparing different divisions along the vertical direction, the results show that if there is no division along the z-direction, the whole solution time increases a lot, which indicates the solution of the submatrix equation is time-consuming for the block containing the high-contrast dielectric interface.

C. Multithread Parallel Computation

To minimize the computational time as much as possible, we use OpenMP as an easy-to-use and simple programming environment for multithread computations to accelerate the FFT. More importantly, regarding the solution to divided submatrix equations of the preconditioner in the iteration [see (10)], the OpenMP instruction is also employed to perform parallel computing. The acceleration of them by the OpenMP is independent of the scheme of precondition. To clarify the effects of the multithread operations on their acceleration, the calculation time with and without the parallelization are compared in Table III. The results show that the multithread operation has a significant impact on the acceleration of the divided submatrix equations

of the preconditioner, which is superior to the acceleration effect on the FFT. Thus, the acceleration by the OpenMP is mainly attributed to the employment of solving independent submatrix equations of the preconditioner.

IV. Conclusion

In this work, the VIE-FFT algorithm combined with a parallel block preconditioned BiCGSTAB method is proposed for modeling the electromagnetic response from nanostructures with two representative examples of focusing metasurfaces and plasmonic solar cells. The preconditioning method employs the block decomposition technique compatible with the geometric features of nanostructures to speed up the iteration, which is suitable for OpenMP parallel implementation on distributed memory architectures. Numerical examples show that wave interaction within nanostructures influences the numerical performances of the preconditioner. The block regions need to be set to capture both far-field interference and near-field coupling effects. Consequently, the iterative steps are significantly reduced by using the developed preconditioner. In future works, expanded blocks containing more field information for nanoelectromagnetic problems are worth investigating.

References

[1] J. Xiong, E.-L. Hsiang, Z. He, T. Zhan, and S.-T. Wu, "Augmented reality and virtual reality displays: Emerging technologies and future perspectives," *Light, Sci. Appl.*, vol. 10, no. 1, pp. 1–30, Oct. 2021.

[2] M. Khorasaninejad and F. Capasso, "Metalenses: Versatile multifunctional photonic components," *Science*, vol. 358, no. 6367, Dec. 2017, Art. no. eaam8100.

[3] S. E. Gledhill, B. Scott, and B. A. Gregg, "Organic and nano-structured composite photovoltaics: An overview," *J. Mater. Res.*, vol. 20, no. 12, pp. 3167–3179, Dec. 2005.

[4] M. J. R. Heck, "Highly integrated optical phased arrays: Photonic integrated circuits for optical beam shaping and beam steering," *Nanophotonics*, vol. 6, no. 1, pp. 93–107, Jan. 2017.

[5] E. M. Mahdy, A. K. Abdelmageed, and E. A. Soliman, "Integral equation formulation for planar plasmonic structures with finite thickness in layered media," *IEEE Photon. J.*, vol. 14, no. 2, pp. 1–9, Apr. 2022.

[6] D. M. Solís, J. M. Taboada, F. Obelleiro, L. M. Liz-Marzán, and F. J. G. de Abajo, "Toward ultimate nanoplasmonics modeling," *ACS Nano*, vol. 8, no. 8, pp. 7559–7570, Aug. 2014.

[7] G. Bachelier, I. Russier-Antoine, E. Benichou, C. Jonin, and P.-F. Brevet, "Multipolar second-harmonic generation in noble metal nanoparticles," *J. Opt. Soc. Amer. B, Opt. Phys.*, vol. 25, no. 6, pp. 955–960, Jun. 2008.

[8] A. Taflove and M. E. Brodwin, "Numerical solution of steady-state electromagnetic scattering problems using the time-dependent Maxwell's equations," *IEEE Trans. Microw. Theory Techn.*, vol. MTT-23, no. 8, pp. 623–630, Aug. 1975.

[9] K. Yee, "Numerical solution of initial boundary value problems involving Maxwell's equations in isotropic media," *IEEE Trans. Antennas Propag.*, vol. AP-14, no. 3, pp. 302–307, May 1966.

[10] J. M. Jin, *The Finite Element Method in Electromagnetics*, 2nd ed. New York, NY, USA: Wiley, 2002.

[11] S. He, W. E. I. Sha, L. Jiang, W. C. H. Choy, W. C. Chew, and Z. Nie, "Finite-element-based generalized impedance boundary condition for modeling plasmonic nanostructures," *IEEE Trans. Nanotechnol.*, vol. 11, no. 2, pp. 336–345, Mar. 2012.

[12] A. M. Kern and O. J. F. Martin, "Surface integral formulation for 3D simulations of plasmonic and high permittivity nanostructures," *J. Opt. Soc. Amer. A, Opt. Image Sci.*, vol. 26, no. 4, pp. 732–740, Apr. 2009.

[13] W.-B. Ewe, H.-S. Chu, and E.-P. Li, "Volume integral equation analysis of surface plasmon resonance of nanoparticles," *Opt. Exp.*, vol. 15, no. 26, pp. 18200–18208, 2007.

[14] S. Kishimoto, S. Y. Huang, Y. Ashizawa, K. Nakagawa, S. Ohnuki, and W. C. Chew, "Transient analysis method for plasmonic devices by PMCHWT with fast inverse Laplace transform," *IEEE Antennas Wireless Propag. Lett.*, vol. 21, no. 5, pp. 973–977, May 2022.

[15] X.-C. Nie, L.-W. Li, N. Yuan, T. S. Yeo, and Y.-B. Gan, "Precorrected-FFT solution of the volume integral equation for 3-D inhomogeneous dielectric objects," *IEEE Trans. Antennas Propag.*, vol. 53, no. 1, pp. 313–320, Jan. 2005.

[16] R. F. Harrington, *Field Computation by Moment Methods*. New York, NY, USA: Wiley, 1993.

[17] Y.-N. Liu, X.-M. Pan, and X.-Q. Sheng, "Skeletonization accelerated MLFMA solution of volume integral equation for plasmonic structures," *IEEE Trans. Antennas Propag.*, vol. 66, no. 3, pp. 1590–1594, Mar. 2018.

[18] H. A. van der Vorst, "Bi-CGSTAB: A fast and smoothly converging variant of bi-CG for the solution of nonsymmetric linear systems," *SIAM J. Sci. Stat. Comput.*, vol. 13, no. 2, pp. 631–644, Mar. 1992.

[19] Z. Q. Zhang and Q. H. Liu, "Three-dimensional weak-form conjugate- and biconjugate-gradient FFT methods for volume integral equations," *Microw. Opt. Technol. Lett.*, vol. 29, no. 5, pp. 350–356, Jun. 2001.

[20] A. Pons, A. Somolinos, I. González, and F. Cátedra, "Fast computation by MLFMM-FFT with NURBS in large volumetric dielectric structures," *Electronics*, vol. 10, no. 13, p. 1560, Jun. 2021.

[21] J. A. Meijerink and H. A. Van Der Vorst, "An iterative solution method for linear systems of which the coefficient matrix is a symmetric M-matrix," *Math. Comput.*, vol. 31, no. 137, pp. 148–162, Jan. 1977.

[22] O. Axelsson, "A generalized SSOR method," *BIT Numer. Math.*, vol. 12, no. 4, pp. 443–467, 1972.

[23] D. Pissoort, E. Michielssen, D. Vande Ginste, and F. Olyslager, "A rank-revealing preconditioner for the fast integral-equation-based characterization of electromagnetic crystal devices," *Microw. Opt. Technol. Lett.*, vol. 48, no. 4, pp. 783–789, Apr. 2006.

[24] M. Carr, M. Bleszynski, and J. L. Volakis, "A near-field preconditioner and its performance in conjunction with the BiCGstab(ell) solver," *IEEE Antennas Propag. Mag.*, vol. 46, no. 2, pp. 23–30, Apr. 2004.

[25] M. F. Catedra, E. Gago, and L. Nuno, "A numerical scheme to obtain the RCS of three-dimensional bodies of resonant size using the conjugate gradient method and the fast Fourier transform," *IEEE Trans. Antennas Propag.*, vol. 37, no. 5, pp. 528–537, May 1989.

[26] Z. Chen and M. M. Ney, "Method of moments: A general framework for frequency- and time-domain numerical methods," in *Proc. Workshop Comput. Electromagn. Time-Domain*, Perugia, Italy, Oct. 2007, pp. 1–4.

[27] Y. Saad and M. H. Schultz, "GMRES: A generalized minimal residual algorithm for solving nonsymmetric linear systems," *SIAM J. Sci. Stat. Comput.*, vol. 7, no. 3, pp. 856–869, Jul. 1986.

[28] P. Sonneveld, "CGS, a fast Lanczos-type solver for nonsymmetric linear systems," *SIAM J. Sci. Stat. Comput.*, vol. 10, no. 1, pp. 36–52, Jan. 1989.

[29] N. Zhao and X. Wang, "A parallel preconditioned bi-conjugate gradient stabilized solver for the Poisson problem," *J. Comput.*, vol. 7, no. 12, pp. 3088–3095, Dec. 2012.

[30] J. A. Kong, *Electromagnetic Wave Theory*. New York, NY, USA: Wiley, 1986.

[31] M. Decker et al., "High-efficiency dielectric Huygens' surfaces," *Adv. Opt. Mater.*, vol. 3, no. 6, pp. 813–820, 2015.

[32] Z. He, J. H. Gu, W. E. I. Sha, and R. S. Chen, "Efficient volumetric method of moments for modeling plasmonic thin-film solar cells with periodic structures," *Opt. Exp.*, vol. 26, no. 19, pp. 25037–25046, Sep. 2018.

[33] W. E. I. Sha, W. C. H. Choy, Y. G. Liu, and W. C. Chew, "Near-field multiple scattering effects of plasmonic nanospheres embedded into thin-film organic solar cells," *Appl. Phys. Lett.*, vol. 99, no. 11, Sep. 2011, Art. no. 113304.